Turing patterns beyond hexagons and stripes

Lingfa Yang, Milos Dolnik, Anatol M. Zhabotinsky, and Irving R. Epstein
Department of Chemistry and Center for Complex Systems, Brandeis University, Waltham, Massachusetts 02454-9110

(Received 17 March 2006; accepted 25 May 2006; published online 27 September 2006)

The best known Turing patterns are composed of stripes or simple hexagonal arrangements of spots. Until recently, Turing patterns with other geometries have been observed only rarely. Here we present experimental studies and mathematical modeling of the formation and stability of hexagonal and square Turing superlattice patterns in a photosensitive reaction-diffusion system. The superlattices develop from initial conditions created by illuminating the system through a mask consisting of a simple hexagonal or square lattice with a wavelength close to a multiple of the intrinsic Turing pattern's wavelength. We show that interaction of the photochemical periodic forcing with the Turing instability generates multiple spatial harmonics of the forcing patterns. The harmonics situated within the Turing instability band survive after the illumination is switched off and form superlattices. The square superlattices are the first examples of time-independent square Turing patterns. We also demonstrate that in a system where the Turing band is slightly below criticality, spatially uniform internal or external oscillations can create oscillating square patterns.
 [DOI: 10.1063/1.2214167]

Turing patterns in reaction-diffusion systems have been proposed as a mechanism for morphogenesis,[1–3] and the Turing instability may play a major role in the generation of skin patterns in a number of animals.[3–5] Early research focused on Turing patterns that arise spontaneously from random initial conditions, which are typically stripes or hexagonal arrangements of spots. Additional patterns—squares and superlattices composed of several simple lattices—have been found in hydrodynamics. These results prompted a search for conditions under which such patterns appear in reaction-diffusion systems with Turing instability. Here we examine two overlapping classes of these patterns: superlattices and squares.

I. INTRODUCTION

Turing's seminal paper[1] on what are now known as Turing patterns triggered the study of pattern formation in nonequilibrium reaction-diffusion systems. Turing patterns are temporally stationary, spatially periodic patterns in reaction-diffusion systems that arise via a saddle-node bifurcation of a spatially uniform steady state that occurs at a finite wave number. This bifurcation is often called the Turing bifurcation. The initial theoretical investigations of the Turing instability were devoted to biological systems, but the first experimental observation of Turing patterns[6] occurred in a chemical reaction-diffusion system almost 40 years after Turing's publication. Since then, most experimental and theoretical studies of Turing patterns have concentrated on simple hexagonal and stripe patterns, which arise spontaneously from random initial conditions in experiments and computer simulations.[7–11]

The search for new Turing patterns also continued, inspired by findings in hydrodynamics, where nonequilibrium macroscopic patterns in autonomous Bénard convection and nonautonomous Faraday waves revealed the existence of novel structures. Square patterns were observed in various versions of Bénard convection, both in experimental and theoretical studies,[12–20] but such configurations were not found in reaction-diffusion systems with Turing instability. It was soon pointed out that a square pattern arising from a supercritical Turing bifurcation is usually unstable to a stripe perturbation in a homogeneous, isotropic, reaction-diffusion system.[21] Also, superlattices were found in experiments with Faraday waves[22–24] and with Bénard convection[25,26] in vertically vibrated fluid layers.

Gunaratne *et al.*[27] were the first to find new geometries of Turing patterns. They demonstrated the existence of rhombic patterns, which represent moderate deviations from hexagonal Turing structures, and, more importantly, they discovered the simplest Turing hexagonal superlattice, the so-called "black eye" pattern. Later, Zhou *et al.*[28] demonstrated that these black eye patterns are not projections of a body-centered cubic structure and suggested instead that they arise from interaction between two layers with different activator diffusion coefficients. On the theoretical side, Judd and Silber[29] have analyzed superlattice Turing patterns formed by interacting square or hexagonal lattices with different wavelengths and spatial phases. Bachir *et al.*[30] have found superlattice patterns in a bistable FitzHugh-Nagumo reaction-diffusion model when the two homogeneously stable states have Turing instabilities with different wave numbers.

Our group has employed the photosensitivity of the chlorine dioxide-iodine-malonic acid (CDIMA) reaction to affect Turing patterns and to create specific initial conditions in order to generate new patterns.[31–38] We have also studied systems of two coupled layers with Turing instability to find out what patterns can arise from their interaction.[39,40] Here we present a review of our recent publications and some new

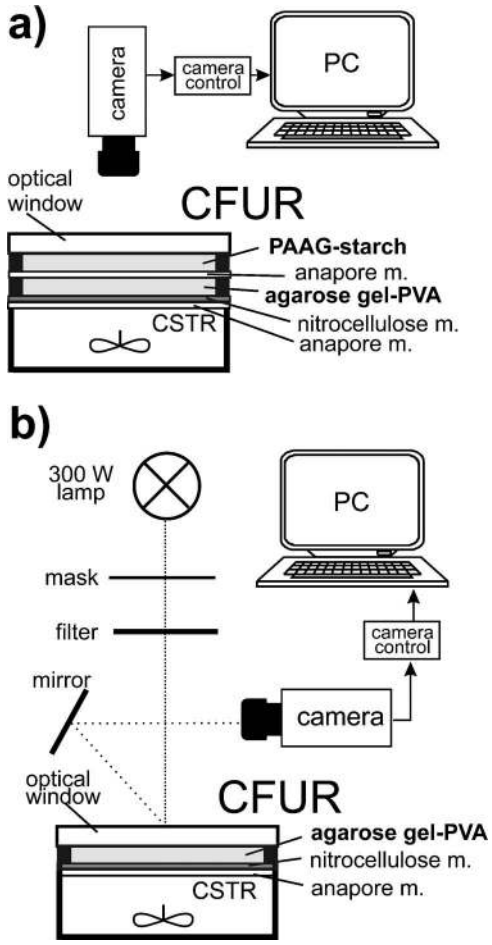

FIG. 1. Schematics of experimental setups. (a) Two-layer system that allows spontaneous formation of superlattice patterns. (b) One-layer system for photochemical induction of superlattices.

results concerning two types of Turing patterns: superlattices and squares.

II. METHODS

A. Two-layer system

The CDIMA reaction was carried out in a one-sided, continuously-fed, unstirred reactor (CFUR) [Fig. 1(a)]. The reactor was thermostated at 4.0 ± 0.2 °C. Two gel layers were placed between a glass optical window and the feeding chamber, a continuously fed stirred tank reactor (CSTR). The feed to the reactor consisted of three solutions, one containing chlorine dioxide, another iodine (Aldrich), and the third malonic acid (MA, Aldrich) and polyvinyl alcohol (PVA, Aldrich, average molecular weight 9000-10000), all in 10 mM sulfuric acid. The residence time of the solution in the CSTR was 230 s.

Above the feeding chamber, we placed an Anapore membrane (Whatman, 0.2 μm pore size, thickness 0.10 mm) impregnated with 4% agarose gel to eliminate stirring effects, and a cellulose nitrate membrane (Whatman, 0.45 μm pore size) to improve contrast. The two gel layers separated by an Anapore membrane were located above the membranes: a 0.3 mm thick 2% agarose (Fluka) gel loaded with 10 g/l PVA immediately above the top membrane, and a 0.3 mm thick polyacrylamide (PAA, Bio-Rad) gel (PAAG) containing 10 g/l starch (Aldrich) solution above the agarose gel.

B. One-layer system with photochemical prepatterning

In this setup, the working medium was a single 2% agarose gel layer (Fluka, thickness 0.3 mm, diameter 25 mm). A nitrocellulose membrane (Whatman, pore size 0.45 μm, thickness 0.12 mm) was placed beneath the gel layer to enhance the contrast of the patterns. To provide rigidity to the system, an Anapore membrane (Whatman, pore size 0.2 μm, thickness 0.10 mm) impregnated with 4% agarose gel was placed between the nitrocellulose membrane and the CSTR chamber. A 300 W quartz halogen lamp was used for illumination. A patterned mask printed on transparent film was placed in front of the light source, and its image was focused on the gel. The mask consisted of a gray-scaled pattern of hexagons or squares. We selected λ_F, the forcing wavelength (wavelength of the mask image projected on the surface of the gel layer), as our control parameter. Two crossed polarizers or different types of neutral density filters were employed to control the light intensity. A Pulnix CCD video camera equipped with a Hamamatsu camera controller was used for image acquisition [Fig. 1(b)]. Snapshots were taken at a light intensity of 0.6 mW/cm^2. In the absence of additional illumination through a mask after the pattern suppression, the iodine concentration replenished itself and the concentration of the starch–triiodide complex gradually increased, giving rise to a new labyrinthine Turing pattern.

III. RESULTS

A. Mechanism of spontaneous formation of black eye patterns in two-layer systems

1. Computational study

Zhou *et al.* suggested that the black eye patterns arise due to interaction of two layers with different activator diffusion coefficients.[28] We investigated this idea by developing a simple model of two interacting layers, each of which exhibits a Turing instability, but with different wavelengths.[39] Each layer contains the same set of reactants with the same kinetics, but the diffusion coefficients within the layers differ considerably. This situation might be realized experimentally if there were a significant difference in the concentrations of fixed ligands[41] between the two layers. The layer with faster diffusion gives rise to the longer wavelength.

We employed a four-variable model with the general form

$$\begin{aligned}
\frac{\partial u_1}{\partial t} &= D_{u_1}\nabla^2 u_1 + \alpha(u_2 - u_1) + f(u_1, v_1), \\
\frac{\partial v_1}{\partial t} &= D_{v_1}\nabla^2 v_1 + \alpha(v_2 - v_1) + g(u_1, v_1), \\
\frac{\partial u_2}{\partial t} &= D_{u_2}\nabla^2 u_2 + \alpha(u_1 - u_2) + f(u_2, v_2),
\end{aligned} \tag{1}$$

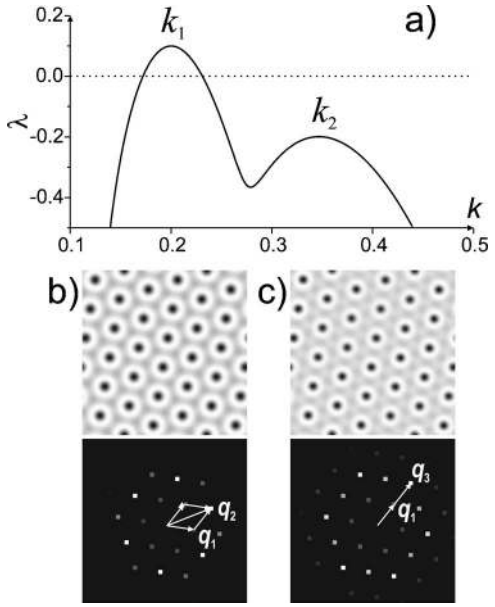

FIG. 2. Emergence of black eye patterns in model (1,2) of a two-layer reaction-diffusion system. (a) Dispersion curve for model (1,2) displaying two Turing bands, one above and the other below criticality. (b) Black eye pattern that develops from random initial conditions; the ratio of moduli of the principal component vectors is $\sqrt{3}:1$. Parameters are $a=3.0$, $b=9.0$, $\alpha=0.1$, $D_{x_1}=16.7$, $D_{y_1}=36.4$, $D_{x_2}=49.5$, $D_{y_2}=117.6$. (c) If the ratio of diffusion coefficients is near 4, patterns emerge with the ratio of moduli of the principal component vectors equal to 2:1. Parameters as in (a) and (b) except: $D_{x_1}=12.6$, $D_{y_1}=27.5$. Periodic boundary conditions, system size 200 $\times$ 200 space units.

$$\frac{\partial v_2}{\partial t} = D_{v_2}\nabla^2 v_2 + \alpha(v_1 - v_2) + g(u_2, v_2),$$

where the reactive species, u and v, and their diffusion coefficients, D_u and D_v, are distinguished by subscripts i, $j=1,2$, that specify the layer. The Laplacian terms describe two-dimensional diffusion within the layers, while diffusional exchange between the layers is represented by the linear coupling terms involving the parameter α. The functions f and g specify the kinetic behavior of the system. We employ two specific models: the Brusselator,[42] with kinetics given by

$$f(u,v) = a - (1+b)u + u^2 v,$$
$$g(u,v) = bu - u^2 v, \tag{2}$$

and the Lengyel-Epstein (LE) model of the CDIMA reaction,[41] with

$$f(u,v) = a - u - \frac{4uv}{1+u^2},$$
$$g(u,v) = b\left(u - \frac{uv}{1+u^2}\right). \tag{3}$$

Figure 2(a) shows a dispersion curve for model (1,2) that displays two Turing bands, one supercritical, the other subcritical. The different positions of the two bands are due to the considerable differences between the diffusion coefficients in the layers. We changed the relevant diffusion coefficients so as to keep constant the wave number of the maximum of the supercritical band while varying the wave number of the maximum of the subcritical band. Figures 2(b) and 2(c) show black eye patterns that develop starting from the uniform steady states with small random perturbations of the variables. When the ratio of diffusion coefficients in the two layers is around 3, black eye patterns arise [Fig. 2(b)] with the ratio of moduli of the principal component vectors equal to $\sqrt{3}:1$, as observed in experiments.[27,28] If the ratio of diffusion coefficients is close to 4, the patterns that emerge show a 2:1 ratio of moduli of the principal component vectors [Fig. 2(c)].

These computational results demonstrate that interaction between two thin layers with large differences in diffusion can lead to spontaneous formation of black eye patterns.

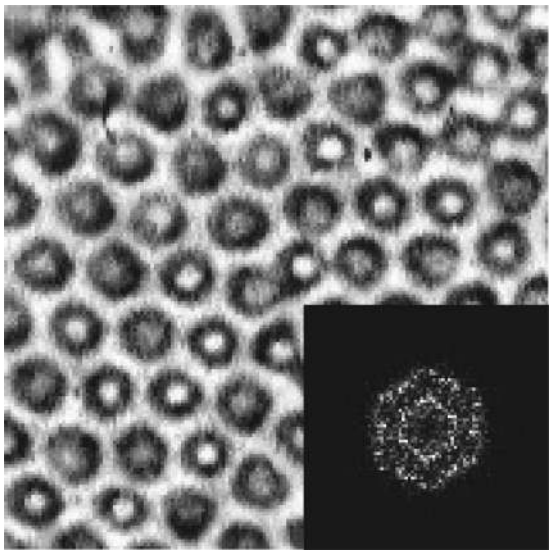

FIG. 3. "White eye" Turing pattern in the two-layer experimental system. The pattern emerges spontaneously at feed concentrations $[I_2]_0=0.36$ mM, $[ClO_2]_0=0.155$ mM, $[MA]_0=1.87$ mM and PVA concentration 1 g/l. Fourier spectrum of the pattern is shown as inset. Frame size is 4×4 mm.

2. Experiment

Gunaratne *et al.*[27] and Zhou *et al.*[28] have obtained black eye patterns in a two-sided CFUR with different initial reactants fed from the two sides, which leads to the establishment of large opposing gradients of the initial reactants. The patterns were attributed to interaction between a polyacrylamide gel (PAAG) layer and a porous glass layer, in which, according to their data, diffusion coefficients are 3–4 times smaller than those in PAAG. We tried to get superlattice patterns in more controlled conditions. We used a one-sided CFUR with weaker, aligned gradients of initial reactants and two adjacent gel layers with drastically different diffusion coefficients for starch and PVA, respectively. In this setting, we obtained a superlattice pattern inverted with respect to the black eye (Fig. 3), which we termed a "white eye."[40] The pattern has been found only in a layer with minimal diffusion of the starch-triiodide complex, a result in accord with our modeling results,[39] where superlattice patterns formed only in the

layer with the shorter wavelength. The pattern in Fig. 3 is not perfectly regular, probably due to spatial nonuniformities in this multilayer system.

B. Emergence of superlattices from simple lattice initial conditions

In our first study of the effects of spatially organized photochemical forcing on Turing patterns, we found that hexagonal patterns of illumination with wavelengths close to the intrinsic wavelength accelerate evolution of the spontaneously occurring, somewhat irregular, hexagonal patterns toward perfect lattices without defects.[34] Later, we examined the effects of subharmonic patterned illumination with ratios of the illumination wavelength to that of the intrinsic pattern near 2.0, 3.0, etc. The most interesting phenomena occur in the middle of the Turing parametric domain, where the width of the Turing instability band is the largest and labyrinthine stripe patterns develop spontaneously. There, photochemically induced concentration patterns of simple hexagonal or square lattices evolve into superlattice patterns after the illumination is switched off.[37]

When the CSTR underneath the gel layer was fed with the reagents of the CDIMA reaction with initial concentrations $[I_2]_0=0.37$ mM, $[MA]_0=1.8$ mM, $[ClO_2]_0=0.14$ mM, and $[PVA]_0=10$ g/l, labyrinthine patterns developed spontaneously. Fourier spectra showed that the wavelength of a stationary pattern, λ_P, was 0.45 ± 0.02 mm. After the labyrinthine pattern was established, the system was brought to a spatially uniform steady state by illumination with uniform light of high intensity (70 mW/cm^2 at the gel surface) from a quartz halogen lamp. As a result of this strong illumination, which was typically maintained for 5 min, the iodine concentration and the concentration of the starch–triiodide complex (responsible for the dark blue color) decreased in the entire illuminated area, and the uniform "white" state replaced the pattern.

After pattern suppression the light intensity was reduced to 23.6 mW/cm^2, a mask was placed between the light source and the reactor, and the image of the mask was focused on the surface of the gel layer. The illumination through the mask was turned off when the photochemically induced pattern became stationary, which typically happened after 30 min of illumination.

1. Hexagonal superlattices

In most cases, we used masks with hexagonal patterns of transparent spots with the transmittance of light through the mask proportional to a sum of sinusoidal functions in the x, y space. The intensity of the light falling on the surface of the gel layer (w) is given by

$$w = W\left\{\left\{\sin\left(\frac{2\pi}{\lambda_F}x\right)+\sin\left[\frac{2\pi}{\lambda_F}\left(\frac{1}{2}x+\frac{\sqrt{3}}{2}y\right)+\frac{\pi}{6}\right]+\sin\left[\frac{2\pi}{\lambda_F}\left(\frac{1}{2}x-\frac{\sqrt{3}}{2}y\right)+\frac{\pi}{3}\right]\right\}\frac{2}{9}+\frac{1}{3}\right\}. \quad (4)$$

Here W is the intensity of the light falling on the gel surface in the absence of a mask. λ_F is the wavelength of the mask image projected on the surface of the gel layer, i.e., the forcing wavelength. Specific values of λ_F were set by changing the distance from the light source to the CFUR while keeping the mask image focused on the surface of the gel layer. We varied the ratio (R) of the forcing wavelength λ_F to λ_P:

$$R = \lambda_F/\lambda_P \quad (5)$$

in the range 0.8–6.0.

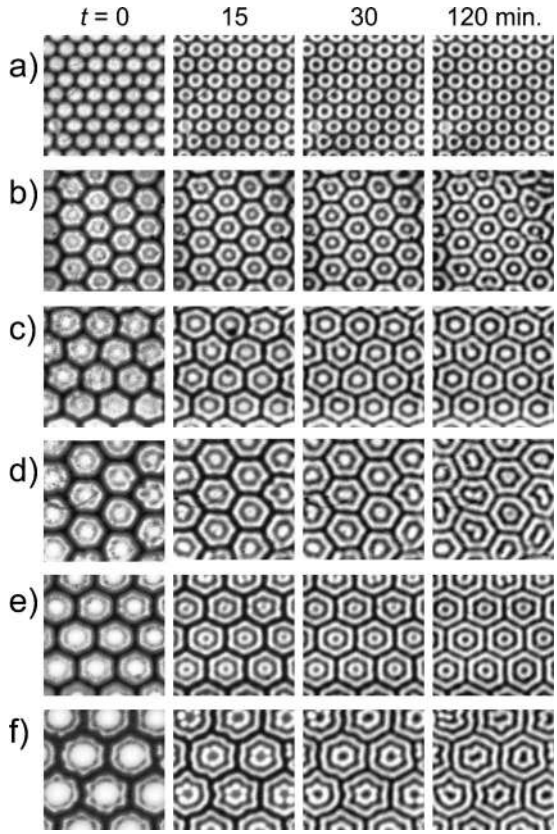

FIG. 4. Development of hexagonal superlattices in experiments with the CDIMA reaction-diffusion system. The initial conditions were created by illumination through transparent spot hexagonal masks with R= (a) 2.0, (b) 2.5, (c) 3.0, (d) 3.2, (e) 4.0, (f) 5.0. The first column displays patterns immediately after the end of illumination through the mask. The numbers above the columns show the time after cessation of illumination. Black corresponds to high concentration of the triiodide-PVA complex. Frame size is 5×5 mm.

Figure 4 shows superlattices induced with hexagonal masks with $R=2.0$, 2.5, 3.0, 3.2, 4.0, and 5.0. The first row shows a black eye pattern. Other superlattices include honeycomb structures containing continuous black lines. Superlattices induced with integer values of R persisted for more than 10 h before slowly beginning to deteriorate. All the superlattices preserved the positions and sizes of the unit cells of the original illumination patterns. Superlattices can be induced for a range of spatial periods of the illumination pattern, i.e., R can deviate significantly from an integer. A superlattice induced with R at or near an integer N displays concentration oscillations along the principal translation axes in which one spatial period contains N maxima. We designate such a pattern superlattice-N. Figures 4(b)–4(d) all show superlattice-3 patterns but superlattices induced with R equal to 2.5 or 3.2 were less stable than those obtained with R

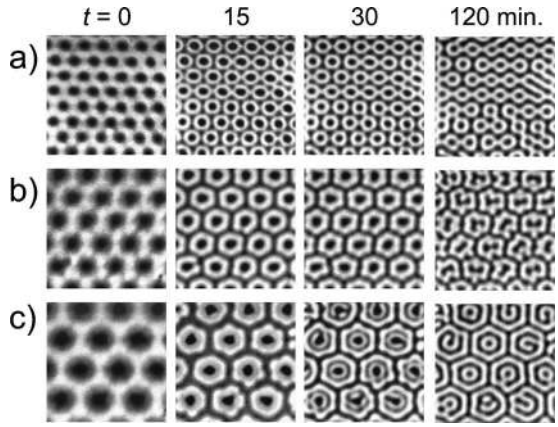

FIG. 5. Development of hexagonal superlattices induced with the opaque spot hexagonal masks with R= (a) 2.0, (b) 3.0, (c) 4.0 in experiments with the CDIMA system. Frame size is 5×5 mm.

=3.0. Defects appeared after 1–2 h, and these superlattices gradually evolved into labyrinthine patterns. Figure 4(f) demonstrates that an illumination pattern with $R=5$ produces an imperfect superlattice-4 with multiple defects, probably due to a zig-zag instability.

Superlattice patterns were also obtained using illumination through inverted hexagonal masks, where the center of each spot is opaque and the area between spots is transparent. Superlattice patterns formed with such masks resemble the superlattice patterns obtained with the corresponding original mask, though the latter patterns display fewer defects. Figure 5 demonstrates the evolution of hexagonal superlattices induced with opaque spot masks. Illumination with $R=2.0$ and 3.0 yielded superlattice-2, while $R=4.0$ generated superlattice-4. These patterns have more defects than the patterns induced with transparent spot masks and soon start to lose the symmetry of the elementary cells.[38]

To analyze the mechanism of generation and the characteristics of these superlattices, we employed a modified LE model:[9,32,41]

$$\frac{\partial u}{\partial t} = a - u - \frac{4uv}{1+u^2} - w(x,y) + \nabla^2 u,$$
$$\frac{\partial v}{\partial t} = \sigma\left[b\left(u - \frac{uv}{1+u^2} + w(x,y) \right) + d\nabla^2 v \right], \tag{6}$$

where $w(x,y)$ represents the effect of the photochemical reaction that consumes I^- and produces ClO_2^- at a rate proportional to the intensity of illumination. As in the experiment, the illumination patterns are hexagonal lattices with the intensity of illumination determined by the sum of three sinusoidal functions chosen so that the minimum intensity is zero. The maximum intensity is designated W, as shown in Eq. (4).

Simulations allow us to follow the development of superlattices in detail and to generate high quality Fourier spectra of the patterns. Figure 6 shows simulations of the evolution of a superlattice-4 from direct and inverted hexagonal illumination patterns with $R=4.0$. The first column shows the illumination patterns, which have the same single spatial frequency. The Fourier spectra in the second column, taken immediately after the end of illumination, reveal that interaction of the photochemical periodic forcing with the Turing instability results in generation of multiple resonant triplets of wave vectors, which are subharmonics of the external forcing. The two illumination patterns generate two different sets of transient spatial harmonics. During evolution of the system after cessation of illumination, only harmonics situated within the Turing instability band grow. The amplitudes of other harmonics decrease drastically, so they are practically invisible in the spectra in the last column of Fig. 6, where the final identical patterns and Fourier spectra are shown.[38]

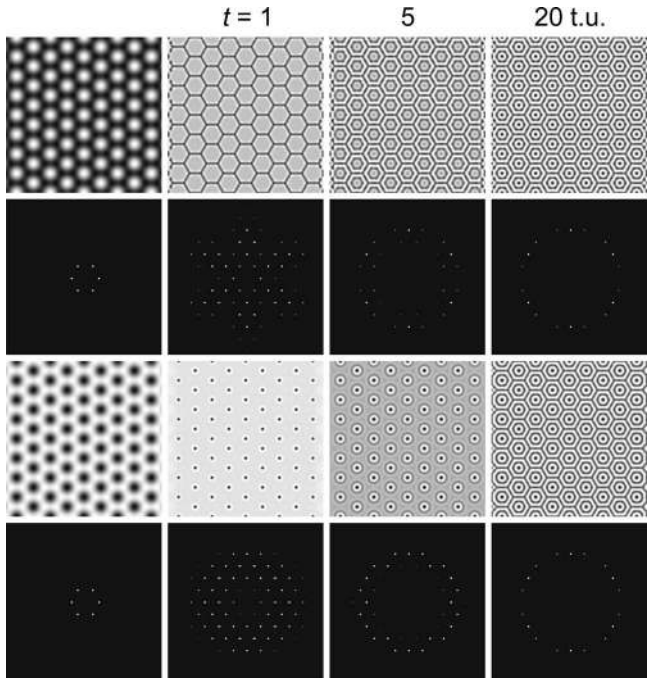

FIG. 6. Simulated development of a superlattice-4 induced by direct and inverted hexagonal illumination patterns with $R=4.0$ and the amplitude of illumination, $W=3.0$ [Eq. (4)]. The first column shows illumination patterns with illuminated spots on a dark background (top row) and opaque spots on an illuminated background (third row). The second column shows the induced patterns and their Fourier spectra almost immediately after the end of illumination. The last column shows the identical stable superlattice-4 patterns. Model (6) with parameters: $a=12$, $b=0.2$, $d=1$, $\sigma=50$. Zero-flux boundary conditions, system size 256×256 space units.

Our simulations showed that illumination patterns with opaque spots always induce superlattices with black central disks, while illumination pattern with transparent spots generate superlattices-2 and -4 with black central disks and superlattices-3 and -5 with white central disks (Fig. 7). Thus, inversion of the illumination pattern leads to inversion of the resulting superlattice at odd N, but makes no difference at even N. This coincides with the experimental results for $N=2$, 3, and 4.

We note that black eye patterns that arise from random initial conditions have ratios of the moduli of the principal wave vectors equal to $1:\sqrt{3}$ in Ref. 27 and $1:\sqrt{3}$ or 1:2 in our computational experiments,[39] while those generated from the hexagonal lattice initial conditions show ratios of $1:\sqrt{3}/2$.[37]

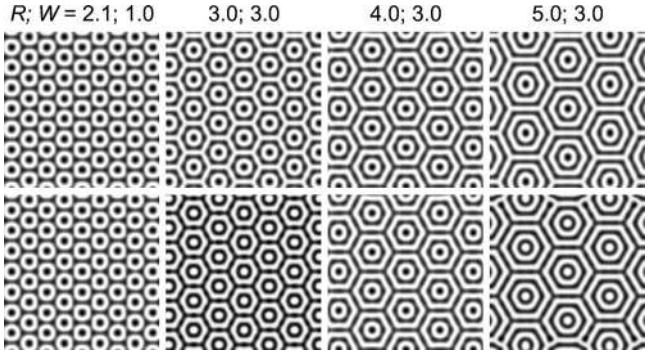

FIG. 7. Parity relations in simulations of illumination patterns and the resulting superlattices. Top row: mask of opaque spots; bottom row: mask of transparent spots. Numbers above the columns show the wavelength ratio, R and the amplitude of illumination, W [Eq (4)]. Model (6) with parameters as in Fig. 6. Zero-flux boundary conditions, system size 128×128 space units.

2. Square lattices

By illuminating the surface of the gel layer with square patterns of transparent spots that had R around 2, 3, and 4 we were able to obtain square superlattices-2, -3, and -4 (Fig. 8).[37] The square superlattices were rather short-lived and evolved into labyrinthine patterns after several hours. When R was 5.0, the pattern that emerged under illumination had a hexagonal elementary cell and evolved to a mixture of stripes and spots within 1 h [Fig. 8(d)].

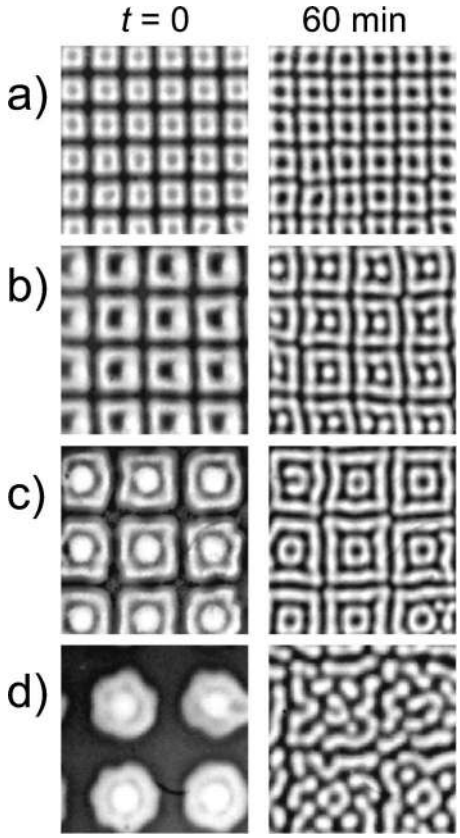

FIG. 8. Square Turing superlattices induced by illumination through square masks of transparent spots in experiments with the CDIMA system. First column shows patterns immediately after the end of illumination through the mask; second column displays patterns 1 h later. R= (a) 2.1, (b) 3.2, (c) 4.3, (d) 5.3. Frame size is 5×5 mm.

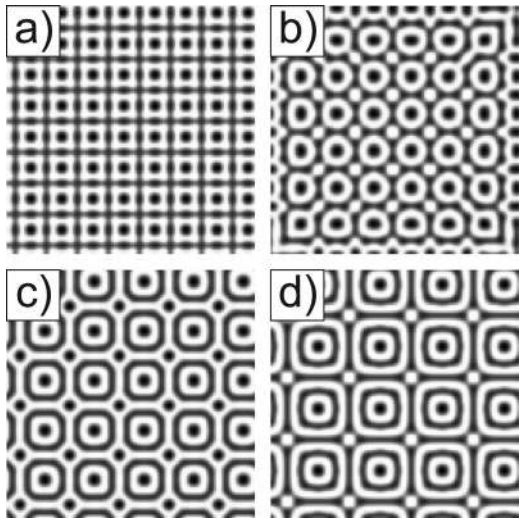

FIG. 9. Square Turing superlattices develop from forced square lattice photochemical patterns in computer simulations. The wavelength ratio, R and the amplitude of illumination, W are (a) $R=2.0$, $W=1.0$; (b) $R=2.4$, $W=1.0$; (c) $R=3.2$, $W=2.0$; (d) $R=4.0$, $W=2.0$. Model (6) with parameters as in Fig. 6. Zero-flux boundary conditions, system size 128×128 space units.

We employed our modified LE model[32] to simulate formation of square Turing superlattices from the forced square lattice photochemical patterns. We obtained superlattices-2 to -4 (Fig. 9), but only superlattice-3 was stable, the others eventually turned into various types of stripe patterns.

3. Stability of superlattice patterns

Previous studies have shown that near the boundaries of the Turing domain simple hexagons are stable, but deeper inside this domain, hexagonal patterns become unstable to stripelike perturbations and are converted to stripe patterns. Still deeper within the Turing domain, stripe patterns undergo the Eckhaus instability, resulting in labyrinthine patterns. The basic square pattern is generally unstable.[8]

We were able to induce superlattice patterns in the central region of the Turing domain, where the spectrum of Turing instability is quite wide, the labyrinthine stripe patterned perturbations are the fastest growing, and the basic symmetric patterns are unstable. In our simulations, all hexagonal superlattices with N from 2.1 to 5.0 and square superlattice-3 were stable under both zero flux and periodic boundary conditions. To confirm their stability, the established superlattices were subjected to global perturbation by small amplitude natural labyrinthine patterns for times an order of magnitude longer than the time of development of the superlattices. After removal of the noise, the perturbed patterns relaxed back to the original superlattices. We also studied competition between labyrinthine patterns and superlattices. We subjected part of a rectangular area to patterned illumination, while the remaining part was not illuminated. During the transition period after switching off the illumination, limited invasion of the labyrinthine pattern into the superlattice region took place. This invasion resulted in formation of a narrow stripe-dot boundary between the two regions, parallel to the original boundary of illumination. After that, some

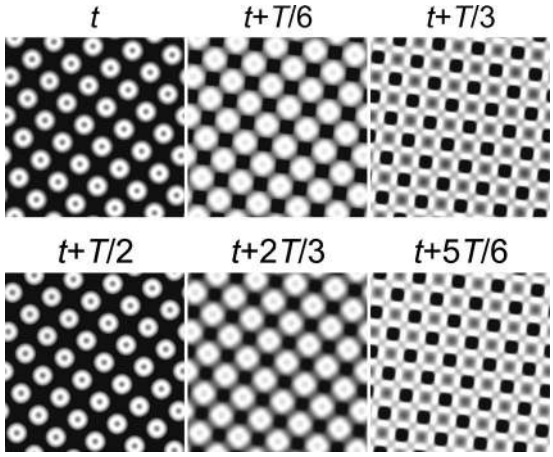

FIG. 10. A stable oscillating square superlattice-2 in the Brusselator reaction-diffusion model when a subcritical Turing band interacts with bulk oscillations. Transformation of the pattern is shown from a black eye to a double lattice of solid squares and back during various phases of the oscillatory cycle. Reaction kinetics is given by Eq. (2). Parameters are $a=3.0$, $b=10.2$, $D_u=6.0$. $D_v=10.0$. Periodic boundary conditions, system size 128×128 space units.

rearrangement took place in the labyrinthine portion of the system, but no further changes occurred in the superlattice pattern.[37]

On the other hand, in the experiments some superlattices persisted for more than 10 h but ultimately deteriorated into labyrinthine patterns. Since the corresponding patterns in the model are stable, we believe that the instability in the experiments arose from imperfections in the experimental system.

C. Square superlattices induced by oscillatory forcing

We have found stable oscillating square superlattices in the Brusselator reaction-diffusion model where a subcritical Turing band interacted with bulk oscillations. The bulk oscillations could originate from the Hopf instability in the autonomous system or from spatially uniform external periodic forcing. In both cases we found the same superlattice-2, which transformed from black eye patterns to double lattices of solid squares and back during various phases of the oscillatory cycle (Fig. 10).[43]

To summarize our results on Turing square patterns, we have found stable square Turing patterns in reaction-diffusion models. In all cases we investigated, however, these patterns were always superlattices. No stable simple square patterns were found.

D. Multistability and coexistence of superlattices

We have generated stable and robust hexagonal superlattices with N from 2 to 5 and square superlattices-3 in our simulations with model (6) using the same set of parameters and various lattice initial conditions (see Sec. III B). This multistability can be employed to create multiple adjacent domains with different geometries and stationary domain walls between them. Here we demonstrate several examples. Figure 11 presents development of coexisting stable domains of square and hexagonal superlattices-3. Figure 12 demonstrates that domains of square superlattice-3 and hexagonal superlattices-2, -3, and -4 can develop simultaneously from suitable initial conditions and form a stable compound pattern with stationary domain walls.

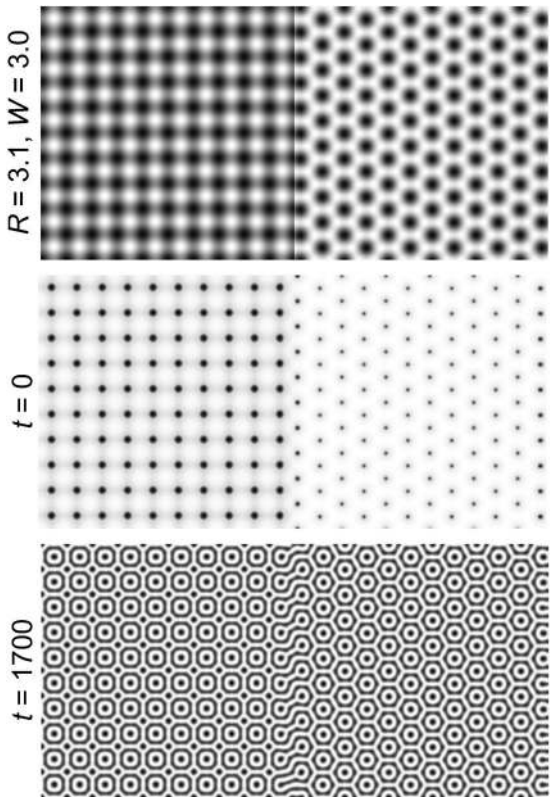

FIG. 11. Coexistence of stable domains of square and hexagonal superlattices-3 in simulations. The top frame shows the illumination pattern, the next frame displays the pattern immediately after the end of illumination and the third frame shows the stable pattern. Model (6) with parameters as in Fig. 6. Zero-flux boundary conditions, system size 512×256 space units.

IV. DISCUSSION

Until recently the only known symmetric stable Turing patterns were hexagonal lattices, parallel stripe patterns and a single superlattice, the black eye pattern. Inspired by the discovery of square and superlattice patterns in Bénard convection, where the basic instability is of the same type as Turing's, we have sought to expand the zoo of symmetric Turing patterns

We have found that, in the CDIMA reaction-diffusion system, illumination patterned as a simple hexagonal or square pattern creates initial conditions leading to development of superlattice patterns that persist for 10 h or more before starting to deteriorate. In computer simulations, we have shown that such a procedure results in formation of stable superlattices in wide ranges of parameters. We have also shown that these superlattices can form coexisting domains separated by stationary domain walls.

The square superlattices are the first examples of time-independent Turing square patterns found in reaction-diffusion models. Recently, Roussel and Wang[44] found a simple square lattice pattern in an excitable version of the Gray-Scott model. They showed that sequential duplication

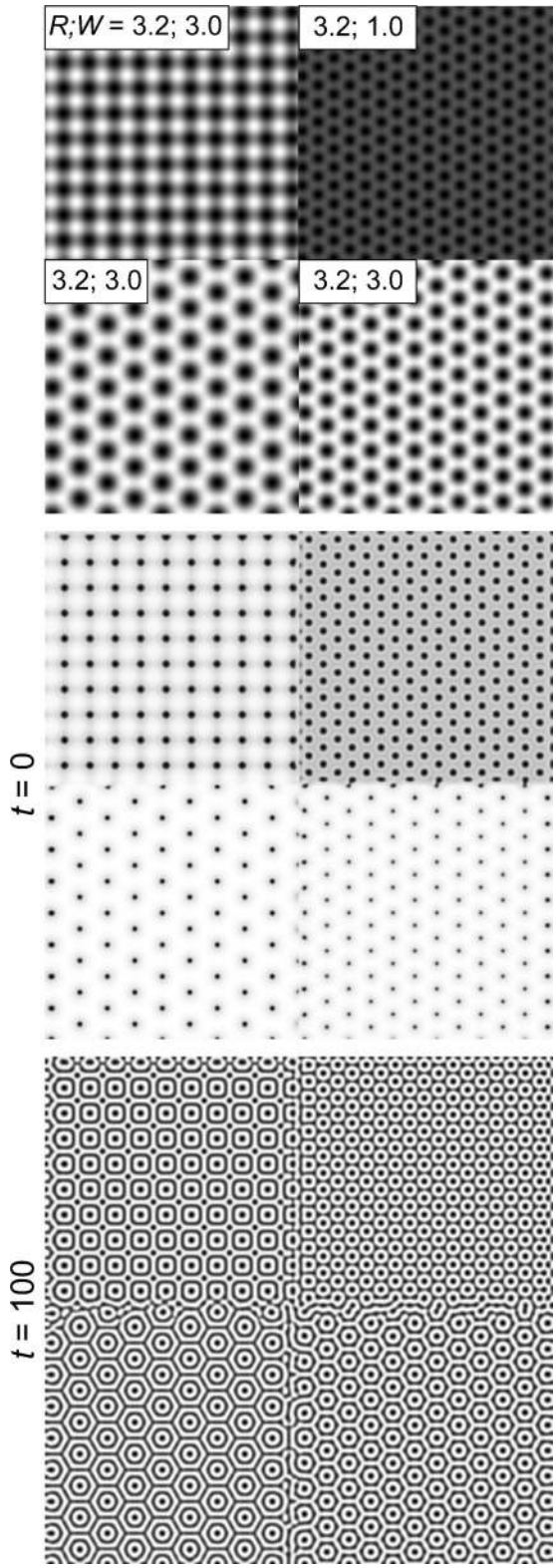

FIG. 12. Coexistence of stable domains of square superlattice-3 and hexagonal superlattices-2, 3, and 4. The frame sequence is the same as in Fig. 11. Model (6) with parameters as in Fig. 6. Zero-flux boundary conditions, system size 512×512 space units.

of a single rectangular spot can lead to development of a long-lived, nearly stationary, simple square lattice in a square system with periodic boundary conditions and length eight times the pattern wavelength. However, when we repeated their simulation for a time five times longer than theirs, the square lattice eventually evolved to a hexagonal lattice. It is known that in small systems a square boundary can stabilize square lattices in models where a Turing bifurcation is supercritical. Still, the fact that the square pattern is a metastable attractor in the Roussel and Wang study points to the possibility of finding truly stable simple square lattices in systems with a subcritical Turing bifurcation.

We have also demonstrated that in a system where the Turing band is subcritical, internal or external spatially uniform oscillations can create oscillating square patterns. Thus, specific initial conditions, internal resonances and spatially uniform periodic forcing of Turing systems can produce a variety of stable symmetric patterns with geometries different from the more familiar ones.

ACKNOWLEDGMENT

This work was supported by Grant No. CHE-0306262 from the National Science Foundation.

[1] A. M. Turing, Philos. Trans. R. Soc. London, Ser. B **237**, 37 (1952).
[2] H. Meinhardt and A. Gierer, J. Theor. Biol. **85**, 429 (1980).
[3] J. D. Murray, *Mathematical Biology* (Springer, Berlin, 1989).
[4] S. Kondo and R. Asai, Nature (London) **376**, 765 (1995).
[5] S. Kondo, Genes Cells **7**, 535 (2002).
[6] V. Castets, E. Dulos, J. Boissonade, and P. De Kepper, Phys. Rev. Lett. **64**, 2953 (1990).
[7] Q. Ouyang and H. L. Swinney, Nature (London) **352**, 610 (1991).
[8] R. Kapral and K. Showalter, *Chemical Waves and Patterns* (Kluwer, Dordrecht, 1995).
[9] B. Rudovics, E. Barillot, P. W. Davies, E. Dulos, J. Boissonade, and P. De Kepper, J. Phys. Chem. A **103**, 1790 (1999).
[10] A. De Wit, Adv. Chem. Phys. **109**, 435 (1999).
[11] P. Borckmans, G. Dewel, A. De Wit, E. Dulos, J. Boissonade, F. Gauffre, and P. De Kepper, Int. J. Bifurcation Chaos Appl. Sci. Eng. **12**, 2307 (2002).
[12] P. Le Gal, A. Pocheau, and V. Croquette, Phys. Rev. Lett. **54**, 2501 (1985).
[13] E. Moses and V. Steinberg, Phys. Rev. Lett. **57**, 2018 (1986).
[14] P. Le Gal and V. Croquette, Phys. Fluids **31**, 3440 (1988).
[15] M. Bestehorn, Phys. Rev. Lett. **76**, 46 (1996).
[16] H. Sakaguchi and H. R. Brand, Europhys. Lett. **38**, 341 (1997).
[17] J. Bragard and M. G. Velarde, J. Fluid Mech. **368**, 165 (1998).
[18] K. Eckert, M. Bestehorn, and A. Thess, J. Fluid Mech. **356**, 155 (1998).
[19] M. F. Schatz, S. J. VanHook, W. D. McCormick, J. B. Swift, and H. L. Swinney, Phys. Fluids **11**, 2577 (1999).
[20] M. F. Schatz and G. P. Neitzel, Annu. Rev. Fluid Mech. **33**, 93 (2001).
[21] P. Borckmans, G. Dewel, A. De Wit, and D. Walgraef, in *Chemical Waves and Patterns*, edited by R. Kapral and K. Showalter (Kluwer, Dordrecht, 1995), p. 323.
[22] H. Arbell and J. Fineberg, Phys. Rev. Lett. **81**, 4384 (1998).
[23] A. Kudrolli, B. Pier, and J. P. Gollub, Physica D **123**, 99 (1998).
[24] H. Arbell and J. Fineberg, Phys. Rev. E **65**, 036224 (2002).
[25] J. L. Rogers, M. F. Schatz, O. Brausch, and W. Pesch, Phys. Rev. Lett. **85**, 4281 (2000).
[26] J. L. Rogers, W. Pesch, O. Brausch, and M. F Schatz, Phys. Rev. E **71**, 066214 (2005).
[27] G. H. Gunaratne, Q. Ouyang, and H. L. Swinney, Phys. Rev. E **50**, 2802 (1994).
[28] C. X. Zhou, H. Y. Guo, and Q. Ouyang, Phys. Rev. E **65**, 036118 (2002).
[29] S. L. Judd and M. Silber, Physica D **136**, 45 (2000).
[30] M. Bachir, S. Metens, P. Borckmans, and G. Dewel, Europhys. Lett. **54**, 612 (2001).
[31] A. P. Muñuzuri, M. Dolnik, A. M. Zhabotinsky, and I. R. Epstein, J. Am. Chem. Soc. **121**, 8065 (1999).
[32] A. K. Horváth, M. Dolnik, A. P. Muñuzuri, A. M. Zhabotinsky, and I. R. Epstein, Phys. Rev. Lett. **83**, 2950 (1999).
[33] A. K. Horváth, M. Dolnik, A. M. Zhabotinsky, and I. R. Epstein, J. Phys. Chem. A **104**, 5766 (2000).

[34]M. Dolnik, I. Berenstein, A. M. Zhabotinsky, and I. R. Epstein, Phys. Rev. Lett. **87**, 238301 (2001).
[35]M. Dolnik, A. M. Zhabotinsky, and I. R. Epstein, Phys. Rev. E **63**, 026101 (2001).
[36]I. Berenstein, M. Dolnik, A. M. Zhabotinsky, and I. R. Epstein, J. Phys. Chem. A **107**, 4428 (2003).
[37]I. Berenstein, L. F. Yang, M. Dolnik, A. M. Zhabotinsky, and I. R. Epstein, Phys. Rev. Lett. **91**, 058302 (2003).
[38]I. Berenstein, L. F. Yang, M. Dolnik, A. M. Zhabotinsky, and I. R. Epstein, J. Phys. Chem. A **109**, 5382 (2005).
[39]L. F. Yang, M. Dolnik, A. M. Zhabotinsky, and I. R. Epstein, Phys. Rev. Lett. **88**, 208303 (2002).
[40]I. Berenstein, M. Dolnik, L. F. Yang, A. M. Zhabotinsky, and I. R. Epstein, Phys. Rev. E **70**, 046219 (2004).
[41]I. Lengyel and I. R. Epstein, Science **251**, 650 (1991).
[42]I. Prigogine and R. Lefever, J. Chem. Phys. **48**, 1695 (1968).
[43]L. F. Yang, A. M. Zhabotinsky, and I. R. Epstein, Phys. Rev. Lett. **92**, 198303 (2004).
[44]M. R. Roussel and J. C. Wang, J. Chem. Phys. **120**, 8079 (2004).